Dual-fuel combustion fundamentals: Experimental-numerical analysis into a constant-volume vessel

Cite as: AIP Conference Proceedings **2191**, 020015 (2019); https://doi.org/10.1063/1.5138748
Published Online: 17 December 2019

Lorenzo Bartolucci, Antonio Paolo Carlucci, Stefano Cordiner, Antonio Ficarella, Vincenzo Mulone, Jérémy Quoidbach, and Luciano Strafella

Dual-Fuel Combustion Fundamentals: Experimental-Numerical Analysis Into a Constant-Volume Vessel

Lorenzo Bartolucci[1], Antonio Paolo Carlucci[2], Stefano Cordiner[1], Antonio Ficarella[2], Vincenzo Mulone[1], Jérémy Quoidbach[3] and Luciano Strafella[2, a)]

[1]*University of Rome Tor Vergata, Department of Industrial Engineering, via del Politecnico 1, Rome, 00133, Italy*
[2]*University of Salento, Department of Engineering for Innovation, via per Arnesano, 73100 Lecce, Italy.*
[3]*HELMo GRAMME, Haute Ecole Libre Mosane - Belgium*

[a)]Corresponding author: luciano.strafella@unisalento.it

Abstract. Dual-fuel combustion has shown high potential for the reduction of emissions (especially nitric oxides and particulate matter) keeping almost unchanged fuel conversion efficiency compared with conventional Diesel engines. However, a deep understanding of the phenomena controlling dual-fuel ignition and combustion processes is still needed to further improving engine behavior especially at low load. To this aim, a combined experimental/numerical approach is proposed in this paper, consisting in a detailed experimental test campaign along with a numerical model to represent and then verify the similarities between engine and chamber local thermodynamics conditions. The design and operation of a tailored experimental setup to study the fundamentals of the dual-fuel combustion process at engine-like operating conditions in optically accessible constant volume combustion chamber is a challenging task. In this paper, similar conditions characterizing the engine operation are represented with a first combustion of a lean air-methane mixture. Then, methane is injected into the chamber to mimic low load engine operation condition in terms of overall equivalence ratio. The oxygen left from the first combustion supports the oxidation of the post-injected methane whose ignition is triggered by a diesel pilot injection. Special care is addressed in characterizing heat and mass losses as well as the mass of methane introduced. During experiments, chamber pressure is measured and thus the evolution of the combustion process is characterized. Numerical simulations, carried out by means of the CONVERGE CFD code, are used to check the charge distribution inside the chamber, and evaluate the local thermodynamic conditions after the gas exchange process. A comparison between the experimental and numerical pressure trace profiles has been performed to validate the numerical model. Results obtained confirm the validity of the proposed approach highlighting the need for a careful calibration of the injection parameters to achieve the target conditions close to the spray injection location.

INTRODUCTION

Dual-fuel combustion is a promising technology. In fact, it allows to couple the characteristics of two different fuels - thus optimizing the combustion process in terms of fuel conversion efficiency and pollutant emissions – taking also advantage in some cases of the production from renewable sources - contributing to the global target of CO_2 reduction [1].

The most popular dual-fuel application involves diesel fuel and methane (or natural gas). Despite the undoubted advantages, some drawbacks still remain unsolved, such as idle and low load engine conditions as well as high load for engine knocking tendency with high natural gas substitution rates [2].

Despite the high number of publications on the behavior of retrofitted compression ignition engines to operate in dual-fuel diesel-methane mode [3, 4, 5, 6, 7], only a few are available analyzing the dual-fuel combustion in optically accessible engines [8, 9, 10] and very few in controlled conditions such as constant-volume combustion chamber [11, 12]. On the other hand, a deeper understanding of the complex phenomena governing the ignition and combustion development in dual-fuel conditions is fundamental in order to optimize charge preparation, in terms of pilot injection

74th ATI National Congress
AIP Conf. Proc. 2191, 020015-1–020015-10; https://doi.org/10.1063/1.5138748
Published by AIP Publishing. 978-0-7354-1938-4/$30.00

settings (pilot injection quantity, timing, rail pressure and multiple injections strategies), injector design (nozzle geometry, injector cone angle) and gaseous fuel supply system characteristics (fumigation, indirect or direct injection). For example, the experimental results on pilot fuel distribution, natural luminosity and chemiluminescence of OH* species shown in [8] and collected operating a single-cylinder optical diesel engine, adapted from a light-duty passenger car, allowed to highlight some aspects of the mechanisms dominating pilot fuel autoignition and mixture combustion development. Relevant outcomes were the following: at low equivalence ratios, the consumption of premixed fuel in the central part of the charge is not achieved, so possibly explaining the increase in unburned hydrocarbon emissions found by many studies in fuel-lean conditions; for higher equivalence ratios, the combustion is dominated by flame propagation.

Furthermore, experimental results obtained in controlled conditions would allow the development of specific models of the dual-fuel combustion process, thus paving the way towards the optimization of the combustion process. However, experimental studies on dual-fuel combustion in controlled conditions are very few: in [11], a study concerning ignition delay of pilot injection in dual-fuel combustion was performed for a wide range of initial temperature and pressure conditions, gas equivalence ratio and mass of pilot injection in a constant volume chamber. In this case, the chamber was heated electrically. However, the chamber did not have any opening allowing optical access to the combustion. Moreover, the pilot injection was performed through an in-line diesel injection pump. In another study [12], the setup, similar to the previous one, consisted in a chamber preheated using heating cartridges. In this case an optical opening allowed to optically access the chamber; however, the charge consisted of fully premixed methanol/air mixture ignited by a diesel injection.

Therefore, in order to understand better the dual-fuel (DF) combustion fundamentals, a new test rig has been designed and developed. In a previous paper [13], the experimental results obtained on the pilot spray development were used in order to evaluate the capability of the spray models in describing the pilot spray penetration in dual-fuel conditions (low fuel amount, low-medium injection pressure). In this paper, further developments of the test rig are described, thanks to which the autoignition of pilot injection and following combustion of methane/air premixed charge can be achieved. In this paper, a combined experimental-numerical procedure is attended in order to characterize the charge distribution of the air/methane/residual gas mixture before the pilot injection.

DESIGN OF THE EXPERIMENTAL TEST RIG

The experimental test rig has been designed to allow for the characterization of the combustion development in diesel-methane DF-like conditions through imaging/optical techniques. In Fig. 1, a sketch of the experimental layout is shown. The Constant-Volume Combustion Chamber (CVCC) is composed of a cylinder of 0.27 L made of Ergal 7075 with a bolted steel flange. The flange has an opening with a quartz window, which allows the combustion to be visualized.

The side surface of the cylinder is characterized by: four seats for glow plugs used to preheat the combustion chamber whenever required (“6” in Fig. 1), one opening for high (fed from the air cylinder) or low (from air compressor “7”) pressure compressed air inlet (“9” in Fig. 1) controlled with the solenoid valve “8” in Fig. 1; one seat for a piezoresistive pressure transducer (“P” in Fig. 1); one opening for the methane inlet (“10” in Fig. 1) controlled with the solenoid valve “4” in Fig. 1; one opening for the exhaust system (“5” in Fig. 1); one opening at the top of the CVCC for a port-fuel methane injector (“3” in Fig. 1); two seats on the sides, one for a K-type termocouple (“T” in Fig. 1) and the other for a spark plug housing a piezoelectric pressure transducer (AVL model ZI21 U3C) (“2” in Fig. 1). Finally, in the center of the rear side, a seat is provided for the diesel fuel injector (“1” in Fig. 1). The characterization of a common rail injector, numerical and experimental, has been reported in a previous works [13].

The piezoresistive pressure transducer labeled as “P” (Keller model PA-21Y) was added for “pegging” the pressure measurement provided by the piezoelectric pressure transducer in “2”.

The heat released by the glow plugs was controlled using the signal provided by the K-type thermocouple (“T” in Fig. 1) as feedback. For this purpose, the thermocouple was connected to an ASCON C1-3000 temperature PID control box.

The thermocouple signal was sampled using a NI 9213 slot, while the pressure signals were sampled using a NI 9215 slot, both connected to a NI cDAQ 9178.

The injector “3” used for the methane is a gasoline six-hole (0.15mm) injector Magneti Marelli 0529/A 03755 F IHP 072; the injection was obtained generating a square wave signal through NI 9401 module and converting it into a PWM signal by a high-switch transistor.

Injector "1" used for the diesel fuel injection is a five-hole (0.170mm) BOSCH injector 0445110266-825; the injection was obtained generating a square wave signal through NI 9401 module and converting it into PWM signal using a suitable realized electronic board [14].

Still referring to Figure 1, the procedure to be attended in order to run a single experiment can be described as follows. After purging and cleaning the CVCC, a lean mixture of air (introduced from "9") and methane (introduced from "10") is obtained, characterized by an air/fuel equivalence ratio λ_1.

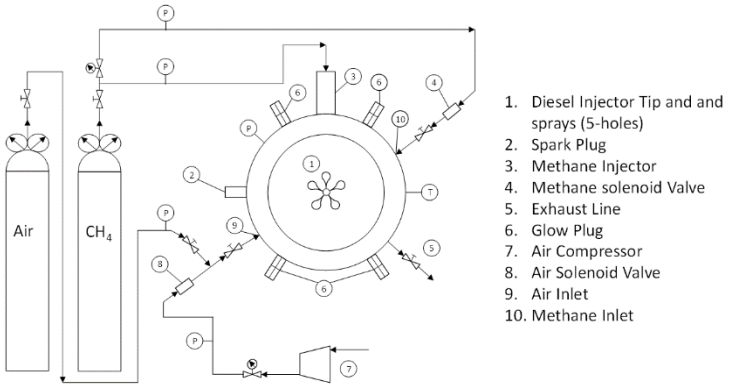

FIGURE 1. Schematic of CVCC setup

The introduced amounts of air and methane can be read from traces reported in Fig. 2 at time equal to 0, representative of all the run experiments. This mixture can be eventually preheated switching on the glow plugs "6". Then, the combustion of this mixture is triggered with the spark plug "2" in the time interval 0-100 ms (see Fig. 2). This leads to a rapid increase of temperature and pressure in CVCC also visible in Fig. 2, together with the consumption of, ideally, all the methane and the related stoichiometric air. The heat exchanged with the CVCC walls cause the temperature and pressure to slowly decrease; the decrease rate is more evident once the combustion of lean mixture of air and methane is ended (right after 300 ms). During this decreasing phase, a second charge of methane is introduced through opening "3" (around 520 ms in Fig. 2); special care is given to perform this injection when the temperature in the CVCC is lower than methane autoignition temperature (~ 550 °C). In this way, a mixture of air/methane/exhaust gases is obtained. Right after, a pilot injection of diesel fuel is injected from "1" (around 650 ms in Fig. 2), when the temperature is still greater than the diesel autoignition temperature (~ 210 °C). The resulting mixture is characterized by an air/fuel equivalence ratio λ_2. In this way, the autoignition of pilot injection triggers the combustion of the above mixture, leading to another pressure increase, evident at 650 ms in Fig. 2).

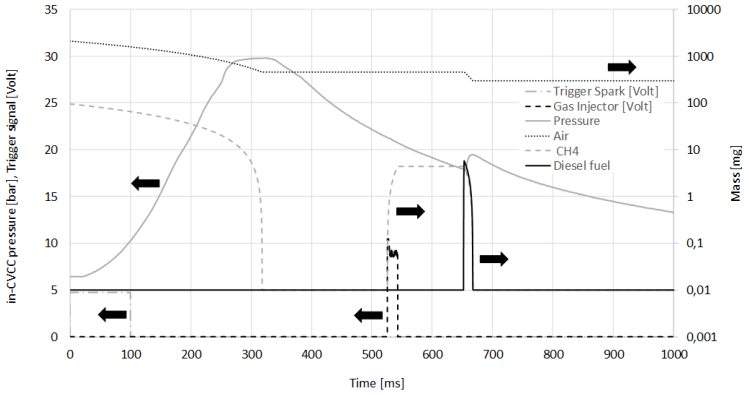

FIGURE 2. In-CVCC pressure, methane and air behavior during DF combustion curve with fraction of species: $\lambda_1 = 1{,}28$ and $\lambda_2 = 2{,}86$

Pressure and temperature evolution in the CVCC before the second combustion event are highly dependent on the development of the first combustion process, which, in turn, depends on the air and methane masses firstly introduced

as well as on the mass leakage and heat transferred to the wall. A careful characterization of all these aspects was therefore performed, as presented and discussed in the following sections.

Chamber Leakage characterization

During the CVCC realization, special care has been addressed in ensuring the best possible sealing of the chamber itself. Therefore, teflon was used to surround the threads and a gas-seal silicone was applied for gas pipes between each fitting. Mass leakage was checked based on specific tests. In Fig. 3, two in-CVCC pressure time histories are reported. The dotted one was measured upon filling the CVCC with compressed air at ambient temperature, while the solid one refers to the cooling phase following one combustion test, performed with CVCC filled with exhaust gases at a temperature higher than ambient (around 1320K, see Fig. 3). The duration of the two reported traces is equal to 1s, which is in the same order of magnitude of the experiments, as reported in Fig. 2. The two traces are equal to almost 25 bar at the beginning of the experiment, and it is thus evident that pressure losses due to mass leakage are negligible if compared with pressure losses due to heat exchanged with the ambient.

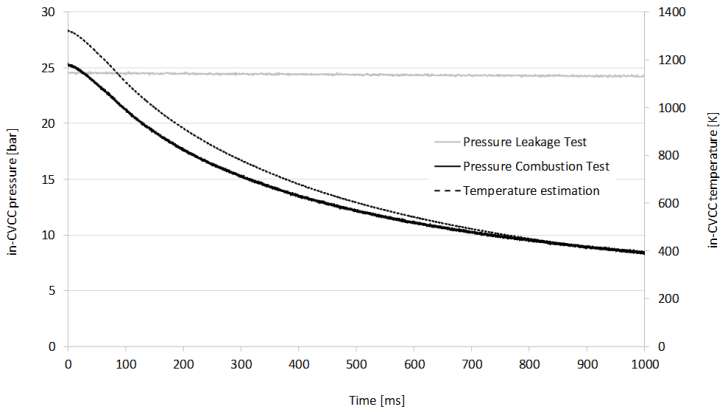

FIGURE 3. Comparison of CVCC conditions (pressure and temperature drop) due to mass leakage only (grey) and and mass leakage + heat exchange (black)

Methane injector characterization

Specific tests were run in order to characterize the methane mass introduced by the injector in the CVCC. The basic idea was to estimate indirectly the mass introduced during one single injection event measuring the related pressure increase into the CVCC through the perfect gas equation of state:

$$m_{CH_4} = \frac{\Delta p \cdot V}{\frac{R}{M_{CH_4}} T} \tag{1}$$

where: m_{CH_4} is the mass of methane introduced during one single injection; Δp is the pressure increase due to the mass introduction; V is the volume of the chamber; M_{CH_4} is the molar mass of methane; T is the temperature in the chamber; R is the ideal gas constant.

The experiments were run as described in the following: the CVCC was first filled with fresh air up to a defined value of chamber backpressure. Then, a series of ten methane injections – all performed keeping constant the methane injection pressure – were carried out using a fixed value of injector energizing time and dwell between consecutive injections. The ten methane injections were controlled and triggered by a LabVIEW Virtual Instrument, while pressure, temperature and injection signals were recorded using a 1 kHz sampling frequency. In-CVCC temperature did not show significant variations respect to ambient temperature after ten injections, therefore the filling process was considered isothermal with very good approximation. On the other hand, the in-CVCC raw pressure trace (shown

in Fig. 4), required a smoothing post processing consisting in the uses of the Savitzky-Golay filter. It is a filter used for data smoothing. This makes the signal more accurate, with no major distortion drawbacks. By convolution, low order polynomials are defined on the basis of a sliding point sample. The resulting smoothed trace is shown in Fig. 4 superimposed to the raw pressure data. On the smoothed trace, relative maxima and minima values are highlighted. Maxima indicate the end of pressure increasing phase due to the introduction of a methane amount corresponding to a single injection event; on the other hand, minima indicate the pressure at the end of mass leakage and just before a new injection event. Therefore, the difference between the pressure values corresponding to a maximum and the consecutive minimum is the pressure increase due to the methane charge corresponding to a single injection event. Based on this value, the mass introduced can be estimated substituting the measured Δp due to every single injection event in Equations (1). This calculation, done for each of the ten injections, allowed to estimate an average mass injected and the related standard deviation.

The above tests were repeated for different values of the controlling parameters, as reported in TABLE 1. In particular, methane injection pressure and chamber back-pressure were varied according to three values, realizing five pressure ratio different conditions. Two energizing times were also tested in order to characterize the mass variation due to injection duration. Finally, two different dwells between injections were also tested in order to highlight the incidence of mass leakage on in-CVCC pressure variation.

TABLE 1. Controlling parameters and relative values varied during tests for methane injection characterization.

Description	Abbreviation	Tested levels
Methane Injection Pressure	x	15 - 25 - 30 [bar]
Chamber Back Pressure	x	10 - 15 - 20 [bar]
Pressure Ratio	PR	1.5 - 1.667 - 2 - 2.5 - 3
Dwell	x	5 - 10 [s]
Injector Energizing Time	ET	20 - 40 [ms]

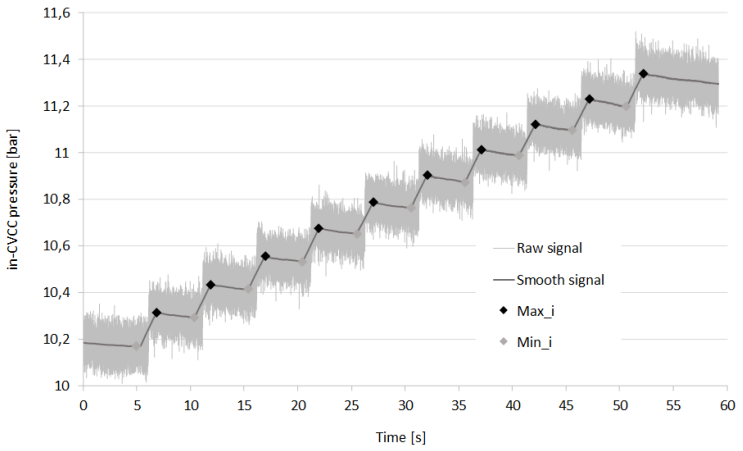

FIGURE 4. Ten methane injections for injector characterization (CVCC back-pressure ≅ 10 bar, methane injection pressure = 30 bar, injector energizing time = 40 ms, dwell = 5 s)

Results of the above tests are grouped in the graph reported in Fig. 5, where the average methane mass is plotted, with its standard deviation, varying the pressure ratio (ratio between methane injection pressure and CVCC backpressure). The average methane mass estimated with an injector energizing time equal to 40 ms was divided by two in order to make it coherent with values obtained at 20 ms. It is possible to observed that, as expected, the mass introduced increases increasing the pressure ratio. The increase is evident at low pressure ratios, while an asymptotic behavior is observed at higher values of pressure ratios. This is coherent with the behavior of the flux behavior through ducts with variable section.

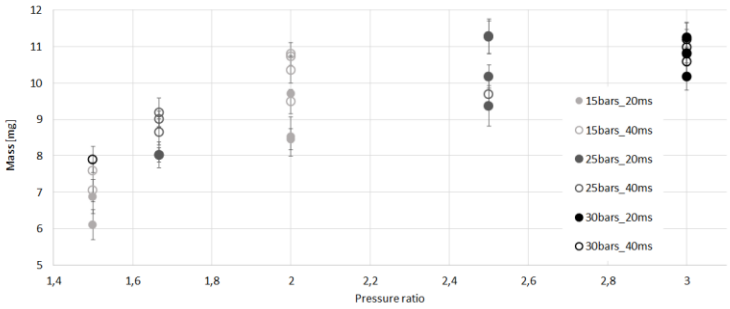

FIGURE 5. Average methane mass - and related standard deviation - introduced at different pressure ratios.

First combustion test

Control of the initial conditions is key to have the correct evolution of the dual fuel combustion process. In the present experimental setup, the initial conditions depend on the combustion of the initial air/methane mixture. The objective of this part is therefore to study the behavior of the first combustion sub-process, composed exclusively of methane and air and ignited by a spark plug. As previously specified, air and methane are introduced into the combustion chamber separately ("9" and "10" in Fig. 1). Furthermore, the amounts of the two gaseous species have to match a target final pressure and air-methane ratio. This latter parameter was controlled measuring the partial pressure related to each specie. Two solenoid valves have been used in order to reach the target final pressure and the related mixture composition.

Special care was addressed in ensuring this first combustion to be reproducible. In fact, knowing and controlling the pressure variation as a function of time due the first combustion sub-process, allows to define methane and diesel injection timings. The pressure - and then temperature - must be high enough when the diesel fuel is injected otherwise its auto-ignition will not occur. Moreover, the longer the time between methane and diesel fuel injection, the better the homogeneity of the methane-air mixture. However, the second methane charge cannot be injected too early or it may either burn during the first combustion or auto-ignite.

Another important parameter is the amount of oxygen remaining after the first combustion. If the amount is too small, the second combustion will not be optimal. The left oxygen can be quantified through air-to-fuel equivalence ratio of the first combustion:

$$\lambda_1 = \frac{\left(A/F\right)_{act}}{\left(A/F\right)_{st}} \tag{2}$$

where $(A/F)_{act}$ is the ratio between air and methane mass actually filling to the combustion chamber, while $(A/F)_{st}$ is the stoichiometric ratio between air and methane fuel, equal 17.24. From this definition, $\lambda = 1$ represents an actual stoichiometric mixture, while $\lambda > 1$ indicates a mixture as leaner as λ exceeds 1. In this work two conditions, namely $\lambda_1 = 1.31$ and $\lambda_1 = 1.12$ have been tested. A higher λ_1 is desired since more air would be available for the second combustion event (DF combustion).

As already described in Fig. 2, the second injection of methane and the pilot injection of diesel fuels take place during the falling phase of in-CVCC pressure, in particular when it assumes values in the range 15-25 bar. From the Fig. 6(a) and (b) it is possible to note that, in the above range, the average in-CVCC pressure well approximate the values measured during the three tests. In fact, the maximum standard deviation is equal to 0.15 bar and 1.07 bar for tests with respectively $\lambda_1 = 1.31$ (Fig. 6(a)) and $\lambda_1 = 1.12$ (Fig. 6(b)). Therefore, even if the combustion curves relating to different repetitions are not identical, they coincide pretty well to the same value after the combustion peak has been reached.

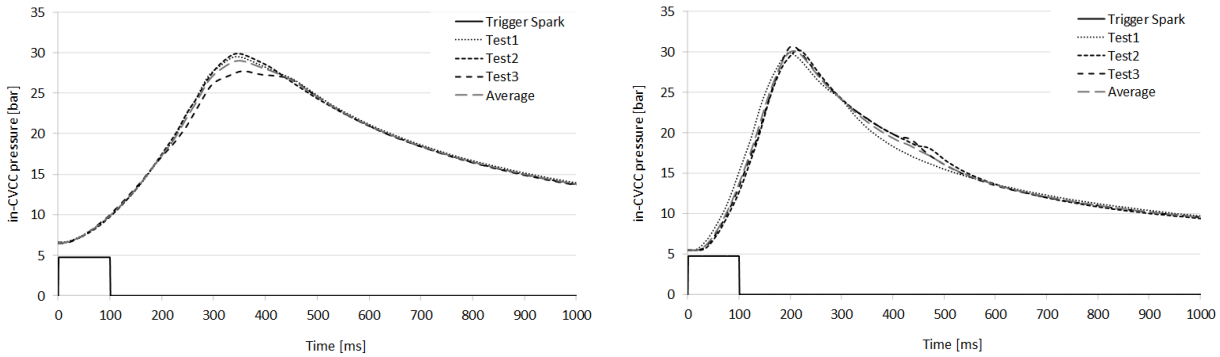

FIGURE 6. Curves with average of the first combustion with $\lambda_1 = 1.31$(a) and $\lambda_1 = 1.12$(b).

Thanks to the pressure curve, it is possible to estimate the ignition delay and combustion duration. Ignition delay corresponds to the time required to obtain a 10% pressure increase of the delta of pressure peak, while combustion duration is defined as the time between the time when the pressure increased by 10% and 90%. The results are reported in the following table. Therefore, it can be concluded that the combustion process is slower for a mixture with $\lambda_1 = 1.31$(a).

TABLE 2. Ignition Delay (ID) and Combustion Duration (CD) for the conditions tested.

Description	**Abbreviation**	**$\lambda_1 = 1.31$**	**$\lambda_1 = 1.12$**
Ignition Delay	ID	37 [ms]	35 [ms]
Combustion Duration	CD	237 [ms]	122 [ms]

Numerical results

The 3D-CFD simulations were carried out with CONVERGE CFD v2.4.26 [15] on the Marconi Cluster at the CINECA facility [16]. The computational domain as well as the monitoring tools were represented accurately in the 3D model (Fig. 7 – top/left) and Adaptive Mesh Refinement together with Fixed Refinement strategies were used to provide high accuracy around the spark plug, the methane injector and in the vicinity of the evolving flame front. Grid size setup was selected according to [13] (Fig. 7 – bottom/right) and the overall cell number was between 105k to 500k. Turbulence was modeled by means of a RANS approach using a k-eps RNG model; calibration constants and parameters were set according to [17]. Thermodynamic initial conditions and information about the energizing time, total injected mass and injection pressure for the methane injection were carefully set to match the experiments. Law of the wall boundary conditions were prescribed for the velocity fields [15]. The combustion process was simulated by means of a detailed chemistry model, using the CSU 186 mechanism already validated for dual fuel combustion in different papers [17-18].

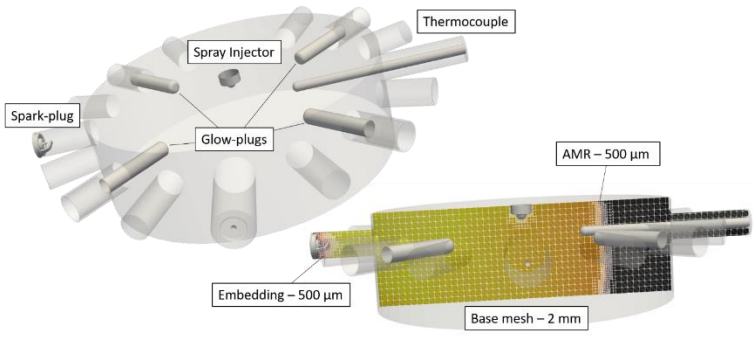

FIGURE 7. Sketch of the simulated domain and of the mesh strategy used for the numerical simulations.

As a first step of the numerical analysis, the focus was posed on the leaner case at λ = 1.31. Particular care was given to the description of heat losses toward the chamber walls. Several simulations were performed looking for a heat convection coefficient capable of representing the heat losses during the whole combustion event. Results, as shown further in the paragraph, provided a good agreement with the experimental data for a convection coefficient in the order of 200 W/m^{2}K with a far field temperature equal to 300 K. Three different gaseous injection tests (namely INJ1, INJ2 and INJ3) were performed focusing on nozzle PR of 1.667 and injecting one to three methane pulses, corresponding to a mass between 8.5 and 25.5 mg (injection duration between 20 and 60 ms). The simulations were performed assuming an ideal rectangular profile for the methane mass flow rate and ensuring the mass matching.

Simulations of the first combustion process were carried out up to 600 ms in order to check the accuracy of the numerical code in matching the evolution of the global thermodynamic parameters inside the CVCC during the methane post-injection event (occurring at 500 ms). The combustion was initiated with a spherical energy source released between the spark-plug electrodes. The energy released was set equal to 800 mJ with a constant release profile to represent the spark event in order to match the first rise of the pressure trace. Results are reported in Fig. 8 in terms of relative pressure as a function of time. The numerical pressure trace is in overall good agreement with the average experimental pressure data and well within the experimental accuracy range attended by the single experiments. The capabilities of the solver of correctly capturing the methane flame propagation and its effects on the evolution of the global thermodynamic parameters were thus confirmed. Moreover, results tell that the assumption of considering the heat losses by a constant convective coefficient appears rather reasonable with a value of 200 W/m^{2}K.

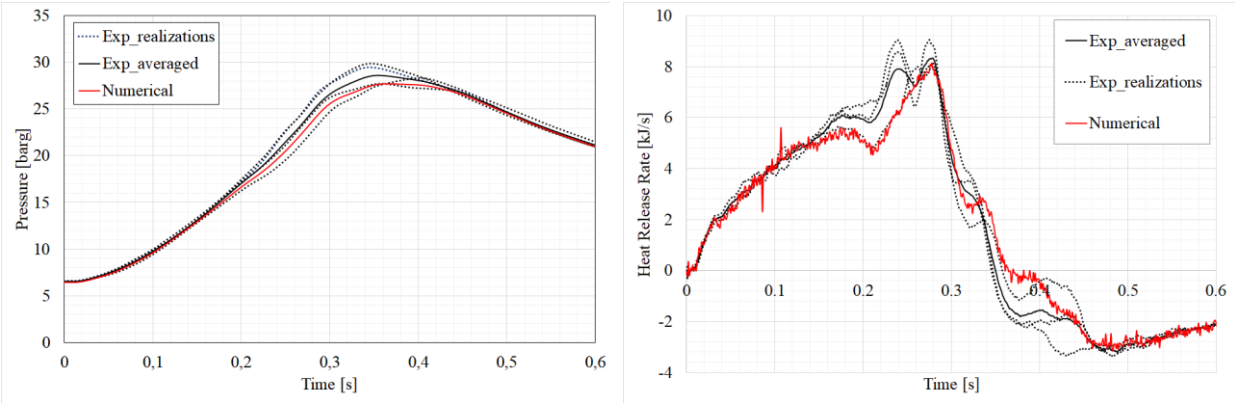

(a) (b)

FIGURE 8. Relative pressure inside the CVCC (a) and AHRR (b) over time, comparison between numerical and experimental data.

At the beginning of the methane injection event, the local thermodynamic conditions are almost homogeneous among the chamber in terms of both temperature and pressure, as well as in terms of species distribution.

Based on the results obtained so far, the analysis of the injection process has been carried out in order to verify the local conditions around the spray injection location before the diesel pilot injection. To this aim, global parameters such as the Uniformity Index (UI) (Equations (3)), the standard deviation of the temperature (T std dev) (Equations (4)) and the averaged equivalent ratio (ϕ avg) were calculated into a cubic volume around the spray injector 100 ms after the start of injection (Fig. 9). In particular, the injection was started at 500 ms and the above mentioned indexes were calculated at 600 ms starting from the beginning of the first combustion event (time zero).

$$UI = 1 - \frac{1}{2n}\sum_{i=1}^{n}\frac{\sqrt{(Y_{CH4} - \overline{Y_{CH4}})^2}}{Y_{CH4}} \tag{3}$$

$$T\ std\ dev = \frac{1}{n}\sum_{i=1}^{n}\sqrt{(T - \bar{T})^2} \tag{4}$$

Results for the three injection cases are reported in Fig. 10. It can be noticed how the INJ 1 case is not able to provide high uniformity of methane and temperature distribution: part of the methane is confined around the injector

location not being able to reach the rest of the volume involved for the spray injection. Poor level of homogeneity can be thus achieved with lean proportions of the mixture. The second injection provides already a good level of uniformity within the control volume both in terms of UI and Temperature standard deviation. Also, the equivalent ratio gets much closer to the target value of 0.25, that is in the same order of magnitude of dual-fuel engines operating at low load with high methane energy substitution [17]. The third injection would ensure greater global uniformity but also an increase of the equivalent ratio due to the greater amount of methane injected.

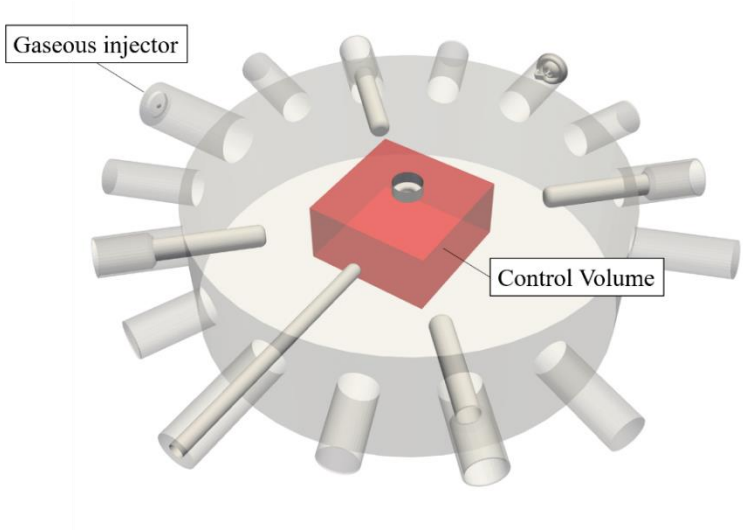

FIGURE 9. Sketch of the control volume (box in red) used of the analysis of the methane post-injection.

It is worth noting that numerical results of the methane injection process are still preliminary, and a complete sensitivity analysis with respect to the main calibration parameters will be presented in a next paper.

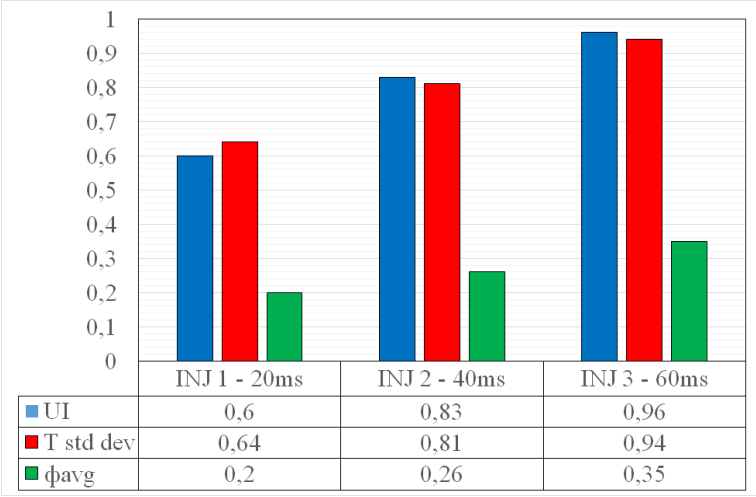

	INJ 1 - 20ms	INJ 2 - 40ms	INJ 3 - 60ms
UI	0,6	0,83	0,96
T std dev	0,64	0,81	0,94
ϕavg	0,2	0,26	0,35

FIGURE 10. Numerical results of the methane post-injection process in terms of uniformity index (UI), temperature standard deviation and overall equivalent ratio averaged within the control volume.

Conclusions

A combined experimental/numerical approach is proposed in this paper, consisting of a detailed experimental test campaign along with a numerical model to represent and then check the similarities between engine and chamber local thermodynamics conditions. In the proposed experimental setup, similar conditions characterizing the engine

operation are represented with a first combustion of a lean air-methane mixture into an optically accessible constant volume combustion chamber. Then, methane is injected to mimic low load engine operating conditions in terms of overall equivalence ratio exploiting the oxygen left from the first combustion. The ignition of this post-injected methane is triggered by a diesel pilot injection. Special care was addressed in experimentally characterizing heat and mass losses as well as the mass of methane introduced. A numerical model was further defined to help characterizing the combustion process in terms of charge distribution and heat losses. The main conclusions of the numerical analysis can be resumed according to the following points:

- The detailed description of the combustion chamber design allowed to represent accurately the behavior of the combustion event in terms of pressure trace;
- A constant value for the heat convection coefficient of 200 W/m^2K was found optimal to represent quite accurately the heat losses towards the wall;
- The injection process analysis highlighted the need for a careful calibration of the injection parameters in order to achieve the target thermodynamic conditions as well as a uniform distribution around the spray injection location;
- Further activities on calibration and analysis of the injection process at different nozzle pressure ratios are required to characterize more extensively this specific experimental setup with respect to the dual-fuel methane-diesel ignition process.

REFERENCES

[1] B. B. Sahoo, N. Sahoo, U. K. Saha, Renew Sust. Energy Rev. **13**, 1151-1184 (2009).
[2] P. Stalhammer, L. Erlandsson, K. Willner, and S. Johannesson, Report SGC 233 (2011).
[3] A. P. Carlucci, A. de Risi, D. Laforgia, F. Naccarato, Energy **33**, 256-263 (2008).
[4] M. Besch, J. Israel, A. Thiruvengadam, H. Kappanna, et al., SAE Int. J. Engines **8** (3), 1342-1358 (2015).
[5] E. S. Guerry, M. S. Raihan, K. K. Srinivasan, S. R. Krishnan, A. Sohail, Appl. Energ. **162**, 99-113 (2016).
[6] K. Poorghasemi, R. K. Saray, E. Ansari, B. K. Irdmousa, M. Shahbakhti, J. D. Naber, Appl. Energ. **199**, 430-446 (2017).
[7] G. Di Blasio, G. Belgiorno, C. Beatrice, Appl. Energ. **204**, 726-740 (2017).
[8] N. Dronniou, J. Kashdan, B. Lecointe, K. Sauve et al., SAE Int. J. Engines **7** (2), 873-887 (2014).
[9] A. P. Carlucci, D. Laforgia, R. Saracino, G. Toto, Energ. Convers. Manage. **52**, 3004-3017 (2011).
[10] A. Carlucci, D. Laforgia, R. Saracino, G. Toto, SAE Technical Paper 2010-01-1297, 2010.
[11] M. Mbarawa, R & D Journal **19** (3) (2003) incorporated into The SA Mechanical Engineer.
[12] C. Yao, J. Hu, Z. Hin, P. Geng, Fuel **174**, 242-250 (2016).
[13] L. Bartolucci, A. P. Carlucci, S. Cordiner, A. Ficarella, D. Laforgia, V. Mulone, V. Rocco, L. Strafella, Energy Proced. **148**, 18-25 (2018).
[14] P. Visconti, P. Primiceri, L. Strafella, A.P. Carlucci, A. Ficarella, International Journal of Automotive and Mechanical Engineering **14**, 3849-3871 (2017).
[15] K.J. Richards, P.K. Senecal, and E. Pomraning. CONVERGE CFD Manual. Convergent Science, 2015.
[16] https://www.cineca.it
[17] Aniello, A., Bartolucci, L., Cordiner, S., Mulone, V., Krishnan, S.R., Srinivasan, K.K. CFD Analysis of Diesel-Methane Dual Fuel Low Temperature Combustion at Low Load and High Methane Substitution. ASME ICEF2018, doi:10.1115/ICEF2018-9649.
[18] Hockett, A. J., Hampson, J., Marchese, A. J. Natural gas/diesel RCCI CFD simulations using multi-component fuel surrogates. Int. J. Powertrains, 2017, Vol. 6.